scientific reports

Check for updates

OPEN

Broadband surface enhanced infrared absorption with multiple Fano resonance by metallic oblique-wire-bundle metamaterial absorbers

Hsueh-Shun Lee[1,4], Yu-Ping Kuang[2,4], Cheng-Yu Lu[1], Ta-Jen Yen[2] & Tsung-Yu Huang[1,3]✉

Higher sensitivity with specific recognition of a sensor could ease the burden of sample purification or labelling procedure for specific testing and detection and there appear two methods including surface enhanced infrared absorption (SEIRA) and surface enhanced Raman scattering (SERS), promising better sensitivity and specificity, simultaneously, via detection of molecular footprints. Furthermore, researchers employ Fano resonance to further boost the detection limit of SEIRA by coupling between two absorption bands from molecules and metamaterials. Still, the current metamaterial absorbers are almost narrow band and require a specific design, only suitable for limited chemicals. Thus, in this work, we would like to design a broadband oblique-wire-bundle (OWB) metamaterial absorber (MA) which could interact with multiple functional groups' absorption from a sample, thus easing the burden of custom-made resonators. In experiments, indeed, our designed OWB MA developed four Fano resonance responses with three PMMAs' functional groups and one function group from carbon dioxide. The counterpart planar MA also performed SEIRA yet without occurrence of Fano resonance as a comparison. We believe this proposed OWB MA could facilitate the development of rapid detection in the field of food safety and chemical detection.

To detect ingredients from an unknown sample with higher sensitivity and specificity is crucial especially regarding food safety and chemical detection. To achieve such a goal, a detection method without labelling procedure should be developed. There appeared many different techniques for detection of chemical structures such as mass spectroscopy, nuclear magnetic resonance spectroscopy, infrared spectroscopy, Raman spectroscopy, etc., and infrared absorption and Raman scattering provide footprints of compositions of a sample and are both applied in so many different fields such as bio-, chemical- and gas-sensors. Besides, signals from both the two methods could be further enhanced through surface modification, also known as surface enhanced infrared absorption (SEIRA)[1–3]and surface enhanced Raman scattering (SERS)[4–6]. The advance of SEIRA and SERS is quick with the development of different nanostructures[7], integration with other materials, e.g., graphene/ graphene oxide, iron oxide, etc[8–13]. , different fabrication procedures for stronger hot spots[14–16], field enhancement from surface plasmon polariton[17,18]and excitation of Fano resonance[3,19]. Among these different methods, one promising kind of SEIRA is to couple a narrow absorption band from molecules' vibration modes to a broadband absorption often introduced by a metamaterial for excitation of Fano resonance that revealed high quality resonance, extended interaction time due to slow group velocity and spectrum reversal for a better signal to noise ratio. To test the performance of Fano resonance based SEIRA substrates, several works have been published, for example, directly printed spiky gold flakes for the coupling between localized surface plasmon absorption and functional groups' absorption from protein–bovine serum albumin with absorbance difference of 8%[16], double Fano resonance based on complementary plasmonic metamaterials and PMMA with a signal strength D_R equal to ~0.3[20], and also an electrically tunable graphene metal hybrid sensor with an electromagnetic introduced transparency like behavior, demonstrating a multiple functional groups' sensing ability[9].

[1]Department of Materials Engineering, Ming Chi University of Technology, R.O.C, New Taipei 243303, Taiwan. [2]Department of Materials Science and Engineering, National Tsing Hua University, Hsinchu 300044, R.O.C, Taiwan. [3]Center for Plasma and Thin Film and Thin Film Technologies, Ming Chi University of Technology, R.O.C, New Taipei 243303, Taiwan. [4]Hsueh-Shun Lee and Yu-Ping Kuang contributed equally. ✉email: huang.tsungyu@mail.mcut.edu.tw

Still, the metamaterial introduced in the above-mentioned methods are narrow bands and only suitable for pre-determined molecular absorption bands, thus limiting their practical use in many different fields. Also, once the absorption peak frequency deviates from the functional groups' absorption frequencies, the sensing abilities of the published sensors were compromised. To tackle this issue, researchers employed strategies such as multiple band metamaterial designs[2], active tunable metamaterials[21], and metal and thickness-dependent metamaterials[22] to enrich the available detection frequency range. However, these methods are insufficient due to their drawbacks such as still limited detection frequency ranges, smaller hot spot areas, difficult fabrication process, and weaker field enhancement. Therefore, in this study, we would like to design an oblique-wire-bundle (OWB) metamaterial absorber accomplished by oblique deposition for its broad absorption band and strong hot spot with larger hot spot areas; with the proposed OWB MA, one might detect a sample composed of a mixture of different kinds of chemicals with a higher sensitivity and a higher signal to noise ratio and without a custom-made sensor.

Fabrication and characterization

Based on our previous work[23,24], we designed an oblique wire bundle (OWB) metamaterial absorber on a silicon substrate with a parallelogram periodicity of $2\,\vec{x}$ and $0.5\,\vec{x}+\vec{y}$ where $|\vec{x}|$ and $|\vec{y}|$ equal to 900 an and 970 nm, respectively. On top of the Si substrate, a 150-nm-thick aluminum and a seed layer of MgF_2 with a base width of 550 nm, a base length of 740 nm, and a thickness of 100 nm are deposited on top of the substrate by sophisticated E-beam lithography and an E-gun evaporator. Note that in experiments, the MgF_2revealed a shape of the frustum of a rectangular pyramid due to the undercut of the resist in the lithography procedure. Then, the sample was put on a stage in an e-gun evaporator with a tilted angle of 86-degree which promised a coverage length of 1430 nm[25], ensuring the growth of metallic nanowires only on top of the seed layer during deposition. Here, to make a comparison, a planar metamaterial absorber with the same periodicity and dimension is fabricated. Note that the thickness of metal in the planar metamaterial absorber is reduced to 50 nm instead of 460 nm, detected thickness of aluminum when fabricating the OWB metamaterial absorber, for better yielding of the lithography process. The entire fabrication procedure of the OWB and planar metamaterial absorbers was detailed in **Methods**. It is worth mentioning that since the OWB metamaterial absorber possessed a broadband absorption spectrum, we expected that the OWB metamaterial absorber could reveal strong Fano resonance without a specific design in advance. Here, to make a comparison, Fig. 1 depicted the schemes and absorbance spectra of the OWB and planar metamaterial absorbers under both the x- and y-polarization incidences from μ-FTIR. The OWB metamaterial absorber possessed a broad absorption band from 100 to 180 THz under x-polarization and an even wider bandwidth 111 THz (69 to 180 THz) under y-polarization incidence. On the contrary, the planar metamaterial revealed an absorption peak of 0.72 with a bandwidth of 15.6 THz under the x-polarization and an absorption peak of 0.6 with a bandwidth of 15.65 THz under the y-polarization. It is worth pointing out that the small peak/dip shown at the frequency of 70.5 THz in the spectra of the OWB and planar metamaterial absorbers could be attributed to the stretching vibration mode of C = O from CO_2. Here, it is an absorption peak in the spectrum of the OWB metamaterial absorber but a dip for the planar absorber, which might stem from the CO_2 concentration variation for the background and device measurement. Still, due to larger hot spot areas and stronger field enhancement, the OWB metamaterial absorber enhanced the vibration mode from CO_2, thus resulting in stronger absorption compared to the planar metamaterial absorber.

To further explore the difference between the OWB and planar metamaterial absorbers, we conducted simulation based on finite integration method with a boundary condition of unit cell along the x- and y-directions and open boundary conditions along the z-direction. Since the MgF_2 is in the shape of frustum, in simulation, its dimensions are modified with a base width and length of 550 and 740 nm and a width and a length of 492.7 and 652.7 nm for the top face. Multiple nanowires with randomly distributed positions, widths, lengths, and thicknesses were generated on top of the seed layer. Indicated by the blue curves of Fig. 1, both the OWB and planar metamaterial absorbers revealed similar absorption bands for the x- and y-polarization between the measured and simulated results. Moreover, from simulation, the absorption bands for the x- and y-polarization incidences started from 85 to 67 THz, respectively, and extended to 384 THz, the upper band edge of the near infrared regime; therefore, our proposed OWB metamaterial absorber revealed bandwidths of 299 and 317 THz under the x- and y-incidences, respectively, which covered almost all the vibrational modes of chemicals for the both polarizations. It is worth mentioning that we expected the OWB metamaterial would reveal stronger absorption and larger bandwidth under the y-polarization incidence due to various optical paths below the metallic wire bundles. Thus, the OWB metamaterial absorber is free from re-design procedure for the detection of most chemicals. In contrast, the planar metamaterial absorber only possessed the limited absorption bandwidth, thus limiting its coupling with molecular vibration modes.

To further characterize the OWB metamaterial absorber and its ability to molecule-plasmon coupled SEIRA, we spin-coated a layer of A5 PMMA on the absorbers with a rotation speed of 1000 rpm for 10 s and then 4000 rpm for 60 s. The expected thickness is around 380 to 460 nm. Here, PMMA possessed three molecular absorption modes within the targeted frequency range, including a C = O stretching mode at 51.9 THz, a CH_2 asymmetric stretching mode at 88.5 THz and a CH_3 stretching mode at 90 THz. Meanwhile, the stretching vibration mode of C = O from CO_2 also existed. As portrayed in Fig. 2, all the four molecular vibration modes could interact with the OWB metamaterial absorber and revealed strong Fano resonance under both the x- and y-polarizations. Note that when PMMA was applied to the metamaterial absorbers, the resonance frequencies of the OWB metamaterial absorber down shifted to the lower range, facilitating a stronger coupling between the stretching vibrational mode of O = C = O from CO_2, indicated by the excitation of the Fano resonance. In contrast, it is difficult to observe the asymmetric line shapes from Fano resonance for the planar metamaterial absorber; instead, the superposition of absorption is observed with larger absorption values at the molecular vibrational frequencies in the spectrum.

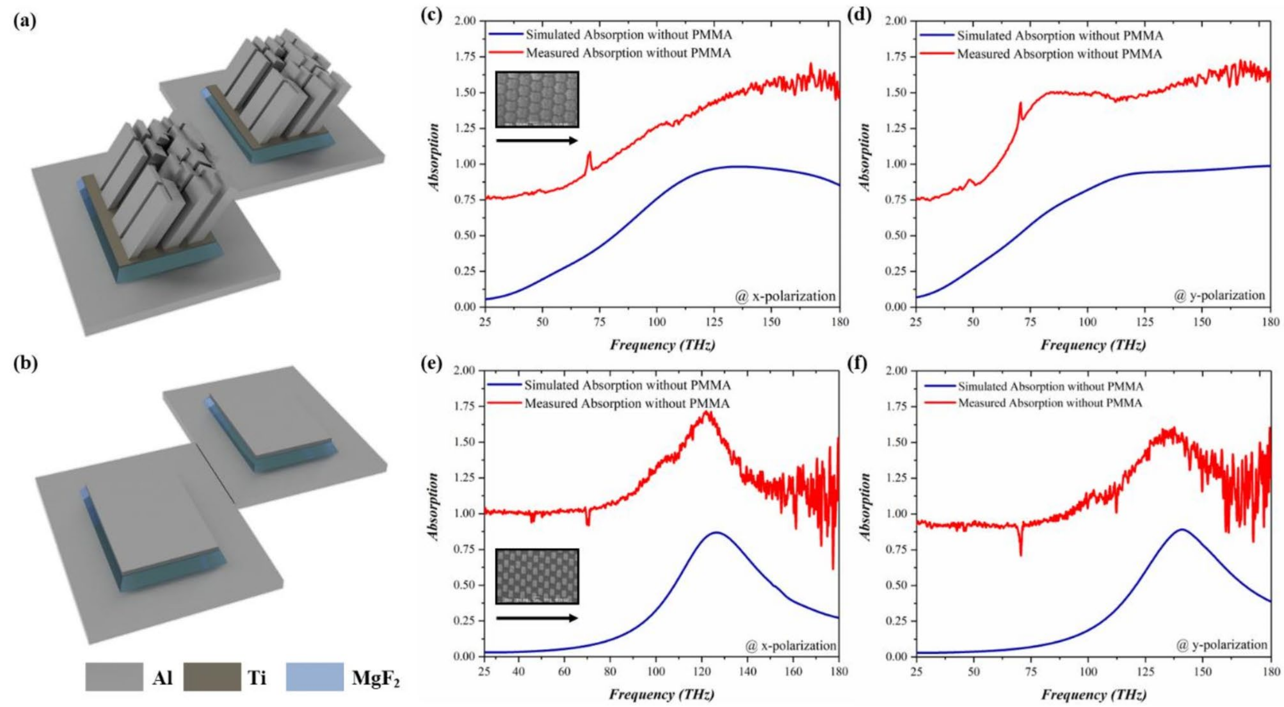

Fig. 1. Schemes of (a) an oblique wire bundle (OWB) and (b) planar metamaterial absorbers. Measured and simulated absorption spectra of (c, d) oblique wire bundle (OWB) and (e, f) planar metamaterial absorbers under the x- and y-polarization incidences without PMMA. Insets show SEM images of the fabricated absorbers. It is worth pointing out that there appeared small peaks in the measured results at 70.5 THz for the spectra of the OWB metamaterial absorber, which could be attributed to the vibrational stretching mode of C = O. These peaks indicated the stronger field enhancement and larger hot spot areas, thus facilitating occurrence of Fano resonance from the OWB metamaterial absorber than the planar one. Note that the absorption dip in (c, d) might stem from the fluctuation of CO_2 concentration for the measurement of the background and the absorber.

Here, to elucidate the interaction between the metamaterial absorbers and chemicals, we conducted simulation of the OWB and planar metamaterial absorbers with PMMA and CO_2 as well. A 460-nm-thick analyte was applied onto the absorber with a dielectric constant predicted by Lorentz model listed below,

$$\epsilon = \epsilon_{b_{Analytes}} + \sum_{j=1}^{4} \frac{f_m \omega_{0,j}^{2}}{\omega_{0,j}^{2} - \omega^{2} - i\gamma_{j}\omega} \tag{1}$$

where $\epsilon_{b_{Analytes}}$ is the relative background permittivity of PMMA and CO_2 and is equal to 2.25, the background permittivity of PMMA, f_m resonance strength of functional absorption groups, $\omega_{0,j}$ the vibrational angular frequency of the functional group and γ_j the damping frequency. Here, to infer the functional group absorption to the analyte, we included three resonance modes from PMMA, i.e., the C = O stretching mode (w_0 = 51.9/g = 0.1 THz), the CH_2 asymmetric stretching mode (88.5/0.7 THz) and the CH_3 stretching mode (90/0.9 THz) and one resonance mode from CO_2, i.e., the C = O asymmetric stretching mode (70.5/0.05 THz). All the resonance strengths are 0.001. From the blue curves of Fig. 2, the OWB metamaterial absorber facilitated occurrence of Fano resonance for all the four vibrational modes with the significant asymmetric line shapes, an indicator of Fano resonance; besides, the signals at the y-polarization incidence are stronger and observable at the 88.5 and 90 THz compared to the ones at the x-polarization incidence, another evidence of better enhancement for the y-polarization incidence. On the other hand, the planar metamaterial absorber only showed Fano resonance for the strongest vibrational mode with the smallest damping, i.e., the O = C = O stretching mode of CO_2 and showed only superposition of absorption for all the other three modes. Still, the hot spots provided by the planar metamaterial absorber could boost the magnitude of absorption when compared to PMMA absorption spectrum with an enhancement factor of around 2 to 3. In addition, the OWB metamaterial absorber revealed profound asymmetric line shapes in experiments compared to the ones in simulation which could be attributed to the hot spots among nano-wire-bundles that are not included in simulation.

For the OWB absorber, under x-polarization incidence at 51.9, 70.5, 88.5 and 90.5 THz, the DR/R_0[3] are 3.07, 1.71, 4.79, and 7.24 times higher when we compared the experimental and simulation results. Also, for the OWB absorber, under the y-polarization incidence at 51.9, 70.5, 88.5 and 90.5 THz, the DR/R_0 are 2.13, 1.33, 1.05, and 1.01 times higher when we compared the experimental and simulation results. As for the planar metamaterial absorber under the x- and y-polarization incidences, the measured results showed 1.47, 0.27,0.85, 0.63 times and

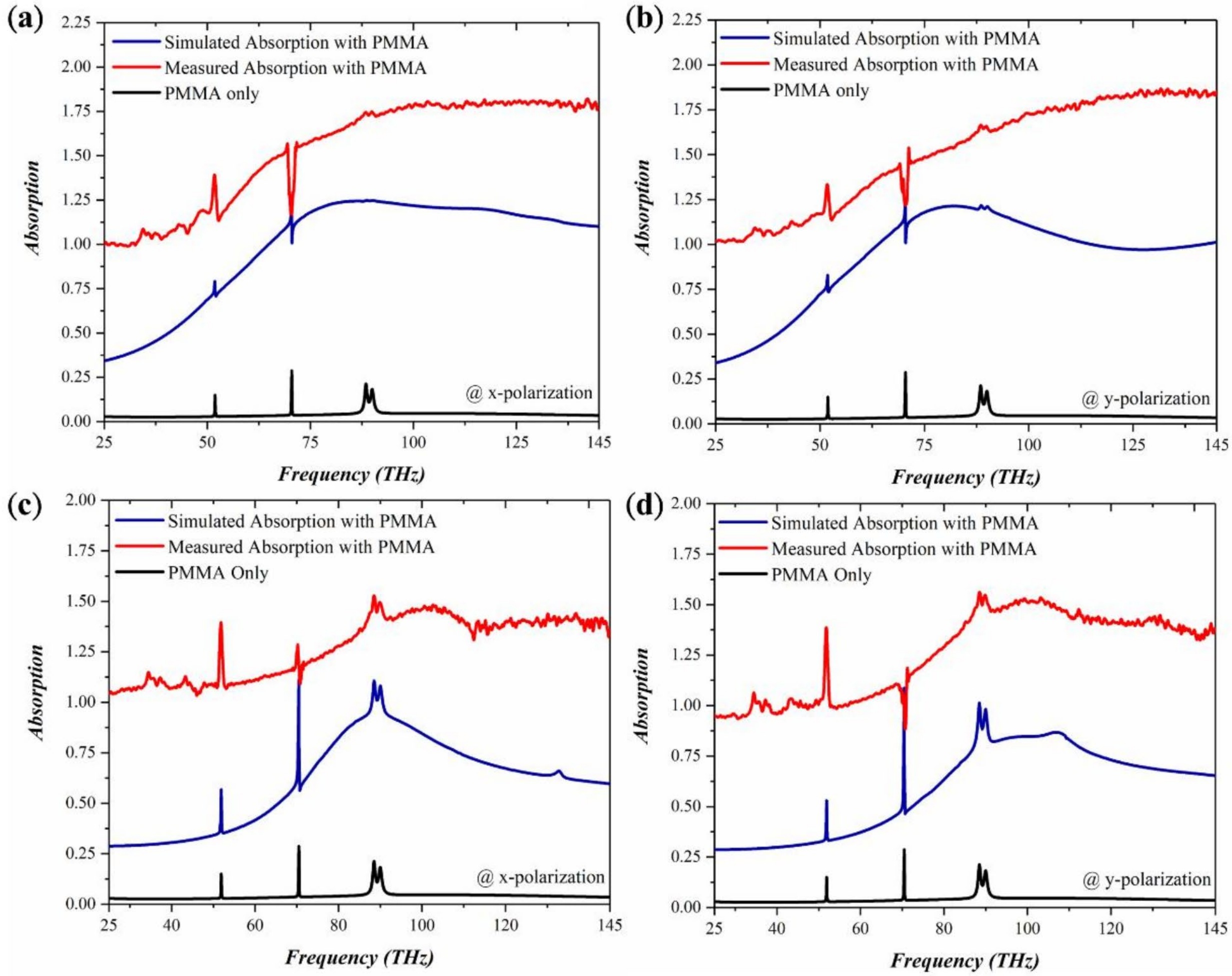

Fig. 2. Measured and simulated absorption spectra of the (a, b) OWB and (c, d) planar metamaterial absorbers under the x- and y-polarizations with PMMA. The OWB metamaterial absorber could couple to all the four molecular vibration modes and developed Fano resonance while the planar metamaterial absorber could only couple to the vibrational mode of CO_2 with a superposition behavior for all the other three modes from PMMA.

2, 0.49, 0.50, and 0.51 times higher DR/R_0 compared to the simulated results. The better enhancement between the measured and simulated results for the OWB metamaterial absorber could be attributed to the hot spots among nanowire bundles, which is not completely considered in the simulation.

To dig out the reasons for better coupling of molecular absorption by the OWB metamaterial absorber, we recorded the absolute field distribution |E| of the two absorbers at the frequency of 126.25 and 140.75 THz as shown in Fig. 3. Note that the chosen frequency was based on the maximum absorption from the planar metamaterial absorber under x- and y-polarizations. For the x-incidence of the OWB absorber, the local highest |E| at the 126.25 THz is 6.32×10^8 while for the y-incidence, the highest |E| at the 140.75 THz is 6.17×10^8, which are both approximately 1.46 times larger compared to the ones of the planar absorber. On the other hand, when considering the global highest |E|, the OWB absorber revealed a value of 6.63×10^8 and 2.16×10^9 for the x- and y-incidence. It is worth noting that the hot spot areas from the OWB absorber are also much larger than the ones of the planar absorber. Also, the maximum |E| differed at the different height of the OWB metamaterial absorber; still, the |E| also varied with respect to the different positions of the y-planes, thus facilitating the sensitivity enhancement for different thicknesses of the analytes.

Furthermore, we would like to discuss two different cases for examining detection ability of the proposed metamaterial absorbers. The first of the two is to reduce the thickness of the analytes, i.e., from 460 nm to 100 nm. The absorption spectra are depicted in Fig. 4(**a**). Again, although small, the OWB metamaterial absorber supported the four asymmetric line shapes as shown in the inset of Fig. 4(**a**). In contrast, the planar metamaterial absorber shows the superposition behavior even for the O = C = O vibrational mode. The other is to reduce the resonance strength of the analyte from 0.001 to 0.0001 while the thickness was maintained. As illustrated in Fig. 5, the OWB metamaterial absorber supported four asymmetric line shapes as shown in the inset of Fig. 5(**a**). In contrast, the planar metamaterial absorber shows the superposition behavior even for the O = C = O vibrational mode.

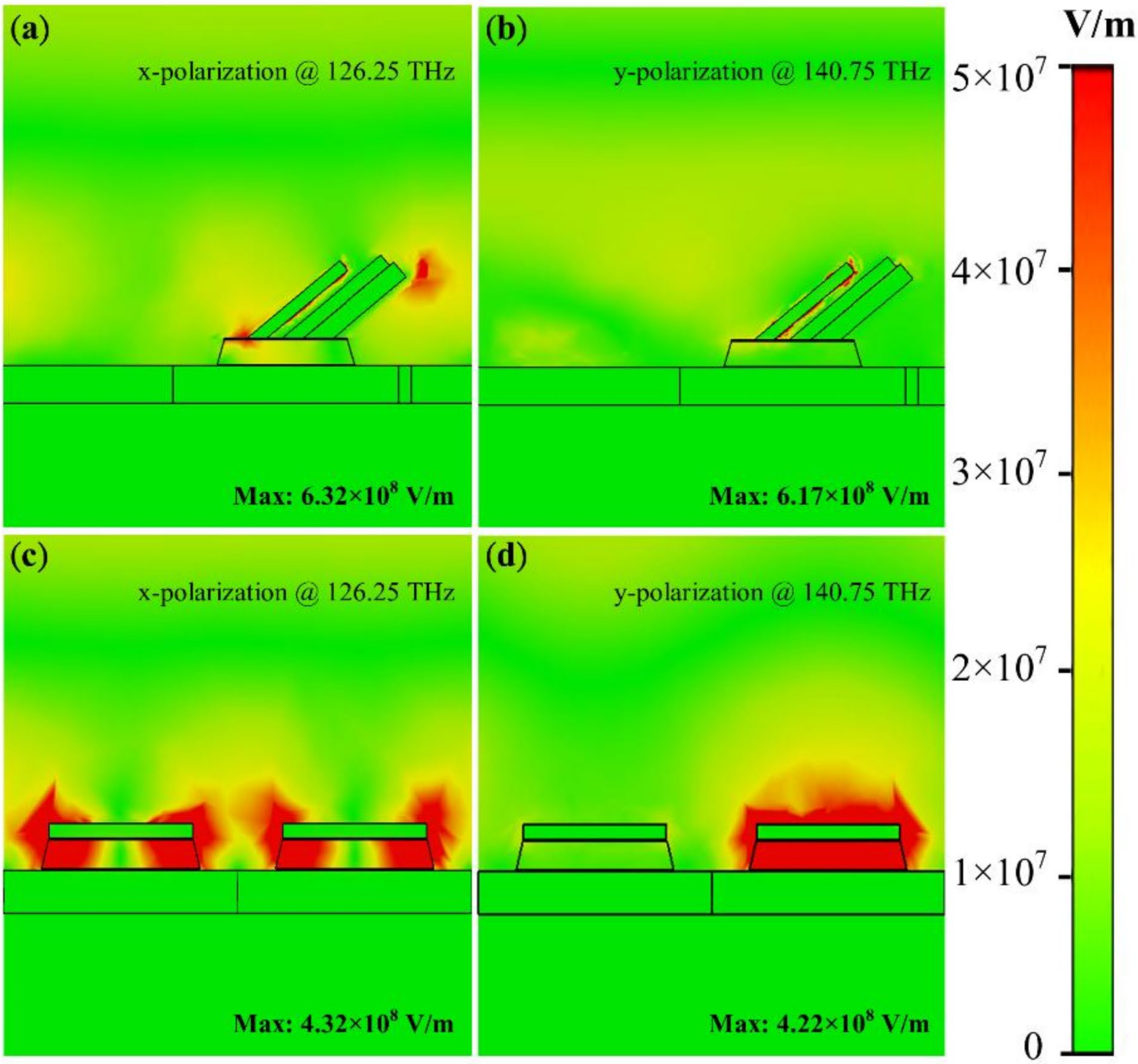

Fig. 3. Absolute field |E| distributions of (a, b) OWB and (c, d) planar metamaterial absorbers under x- and y-polarizations at 126.25 and 140.75 THz, respectively. The OWB metamaterial absorber revealed larger local maximum |E| compared to the ones of planar metamaterial absorber. Moreover, OWB metamaterial absorber showed much more hot spot area compared to the planar metamaterial absorber (not shown here). Also, the global maximum |E| for the OWB and planar metamaterial absorbers are $6.63 \times 10^8/2.16 \times 10^9$ and $4.89 \times 10^8/4.43 \times 10^8$ V/m under x- and y-incidences, respectively, evidencing that the OWB metamaterial absorber indeed provided stronger hot spots with a larger area, facilitating coupling with molecular absorption and occurrence of Fano resonance.

Finally, to reinforce the detection ability of our proposed OWB metamaterial absorber, we plotted the DR with respect to different strengths of PMMA ranging from 0.1 to 0.00001, i.e., different concentrations at the three frequencies for the functional group absorption as shown in Fig. 6. Under the logarithm-logarithm plot, we could observe that all the curves revealed a characteristic of exponential decay. Furthermore, due to the strongest absorption for the O = C = O, the DR was the highest for the polarizations. Also, the DR would saturate once the resonance strength increased. From Fig. 6, all the DR started to saturate at a resonance strength of 0.01 for the two polarizations. Note that since the absorption is weaker for the CH_2 asymmetric stretching modes, the smaller resonance strength (i.e., below 1×10^{-3}) was not enough to excite Fano resonance.

Conclusions

In this work, we have proposed an oblique-wire-bundle metamaterial absorber with broad absorption bandwidths of 299 and 317 THz under the x- and y-polarization incidences, respectively, which covered almost all the infrared absorption spectra of different chemicals. Such proposed OWB metamaterial absorber alongside

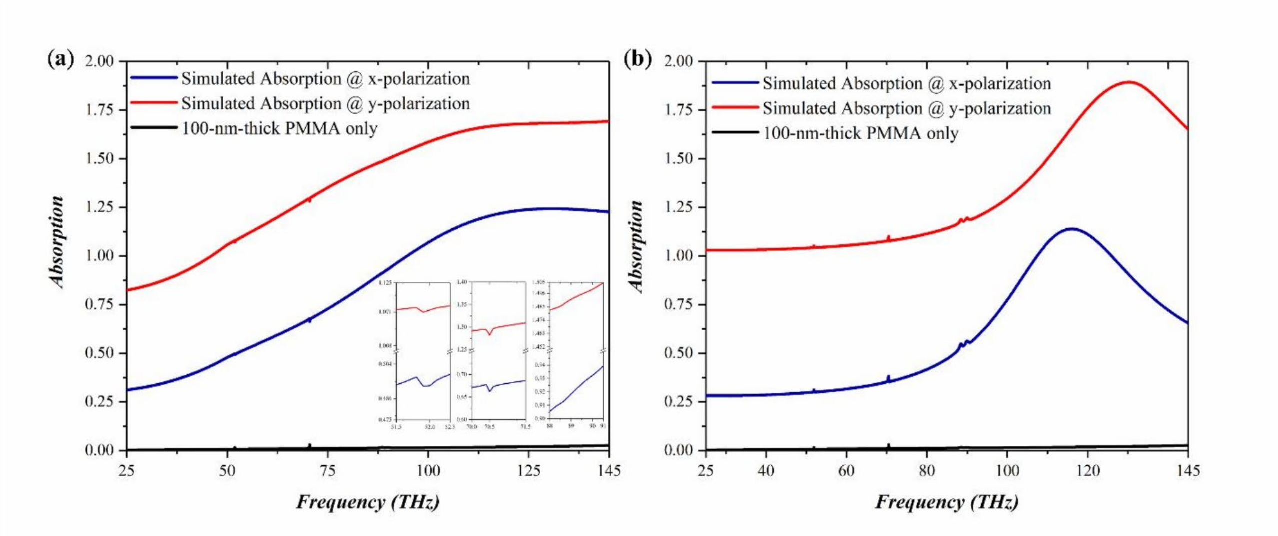

Fig. 4. Simulated absorption spectra of the (a) OWB and (b) planar metamaterial absorbers under the x- and y-polarizations with 100-nm-thick PMMA. The OWB metamaterial absorber could couple to all the four molecular vibration modes while the planar metamaterial absorber only showed the superposition of absorption magnitude even for the O = C = O stretching vibrational mode of CO_2.

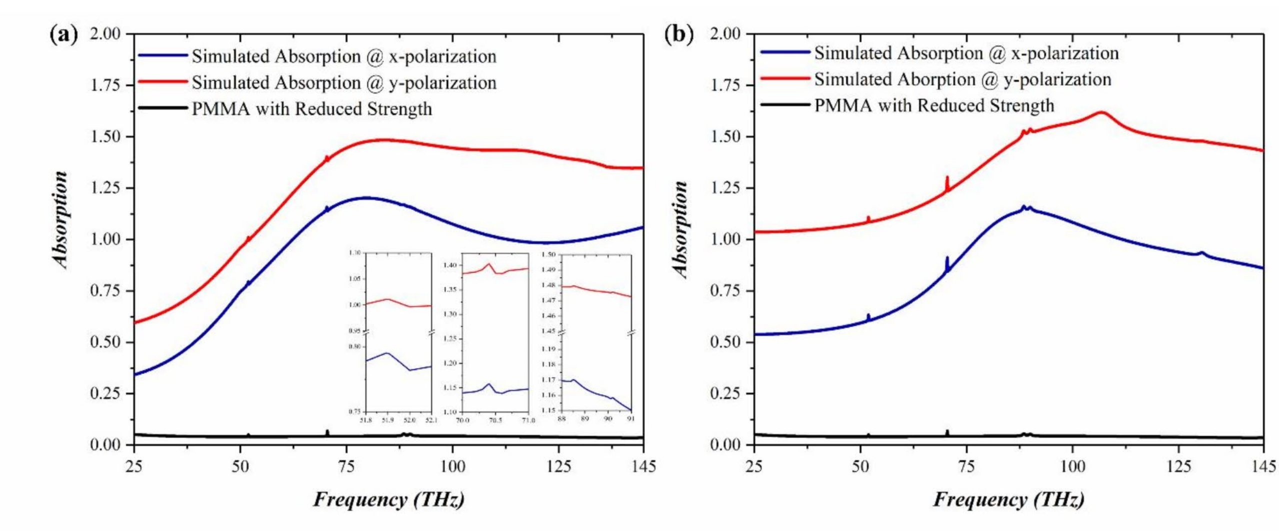

Fig. 5. Simulated absorption spectra of the (a) OWB and (b) planar metamaterial absorbers under the x- and y-polarizations with PMMA for the reduced resonance strength of 0.0001. The OWB metamaterial absorber could couple to all the four molecular vibration modes with the asymmetric line shapes while the planar metamaterial absorber only showed the superposition of absorption magnitude.

with the planar metamaterial absorber are tested with PMMA and CO_2 for the coupling with the vibrational modes of the different analytes. The OWB metamaterial absorber revealed strong interaction with the analytes even with smaller thicknesses or weaker resonance strengths; in contrast, the planar metamaterial absorber could not interact with the chemicals well and showed superposition of absorption for almost all the cases. We believed that this proposed OWB metamaterial absorber could help the development of rapid detection in the field of food safety and chemical detection.

Data availability

The data sets used and/or analyzed during the current study are available from the corresponding author on reasonable request.

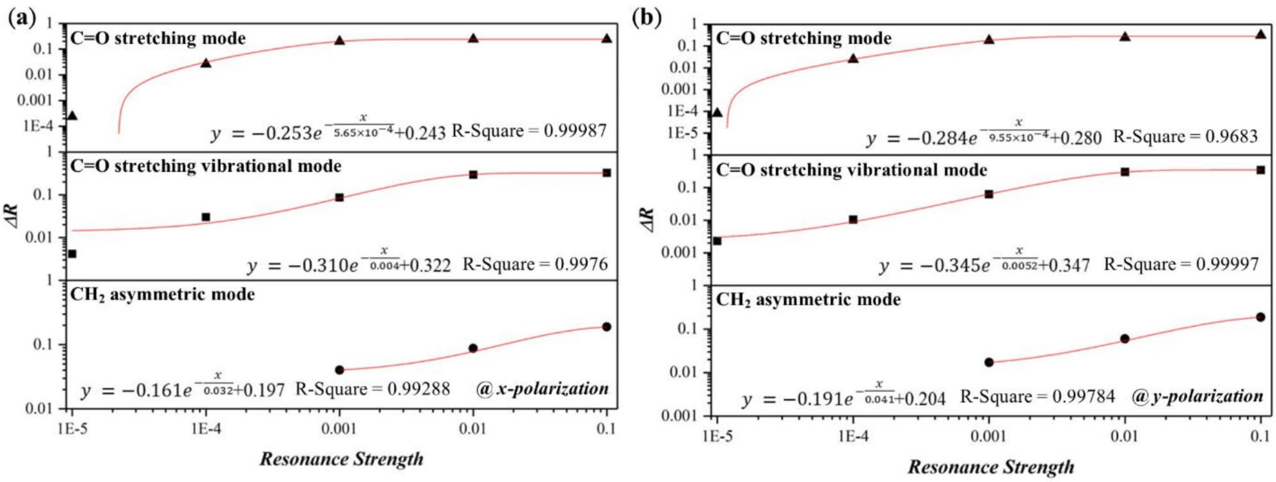

Fig. 6. Schemes of DR with the different resonance strengths for three different functional groups under the (a) x-polarization and (b) y-polarization incidences. The data points could be fitted by exponential decay with R-squares above 0.96.

Fabrication

To fabricate the oblique-wire-bundle metamaterial absorber and its comparison, i.e., the planar metamaterial absorber, we deposited 4-nm-thick titanium and 150-nm-thick aluminum on a silicon substrate. Then, spin coat photo resist of PMMA A5 with an initial rotation speed of 1000 rpm for 10 s and a final rotation speed of 4000 rpm for 60 s. Next, the sample was hard baked under 180 °C for 3 min. In the following, the electron beam exposure was carried out. After exposure, the sample was immersed into a solution of MIBK and IPA in a ratio of 1 to 3 for 50 s. In addition, 120-nm-thick magnesium fluoride was deposited onto the sample. In the following, to fabricate the oblique-wire-bundle metamaterial absorber, the as-fabricated sample was put into acetone for the lift-off process to remove residual photoresist; e-gun deposition was then conducted for 4-nm-thick titanium and for the growth of aluminum wire bundles on an 86-degree tilted stage. On the other hand, to fabricate the planar metamaterial absorber, 4-nm-thick titanium and 50-nm-thick aluminum were consequently deposited onto the sample. Finally, the as-fabricated sample was put into acetone for the lift-off process to remove residual photoresist.

Received: 19 August 2024; Accepted: 4 November 2024
Published online: 09 November 2024

References

1. Autore, M. et al. Boron Nitride nanoresonators for phonon-enhanced molecular vibrational spectroscopy at the strong coupling limit. *Light Sci. Appl.* **7**, 17172 (2018).
2. Dayal, G., Chin, X. Y., Soci, C. & Singh, R. High-Q Plasmonic Fano Resonance for Multiband Surface-enhanced infrared absorption of Molecular Vibrational sensing. *Adv. Opt. Mater.* **5**, 1600559 (2017).
3. Lin, C. T., Yen, T. J. & Huang, T. Y. PVC Detection through a hybrid SEIRA substrate and refractive Index Sensor based on Metamaterial Perfect absorbers. *Coatings*. **11**, 789 (2021).
4. Lee, B. S., Lin, D. Z. & Yen, T. J. A Low-cost, highly-stable surface enhanced Raman scattering substrate by Si Nanowire Arrays Decorated with au nanoparticles and au backplate. *Sci. Rep.* **7**, 4604 (2017).
5. Wang, H., Kundu, J. & Halas, N. J. Plasmonic nanoshell arrays combine surface-enhanced vibrational spectroscopies on a single substrate. *Angew. Chem. Int. Ed.* **46**, 9040–9044 (2007).
6. Fan, X. et al. Three-dimensional SERS sensor based on the sandwiched G@AgNPs@G/PDMS film. *Talanta*. **233**, 122481 (2021).
7. Xia-Hou, Y. et al. Graphene Coated Dielectric Hierarchical Nanostructures for highly sensitive Broadband Infrared sensing. *Small.* **19**, e2206167 (2023).
8. Zeng, K. et al. Synthesized complex-frequency excitation for ultrasensitive molecular sensing. *eLight*. **4**, 1 (2024).
9. Durmaz, H. A graphene-metal hybrid biosensor for SEIRA spectroscopy applications. *Opt. Commun.* **550**, 130020 (2024).
10. Li, J. et al. Ultrasensitive Plasmon-enhanced Infrared Spectroelectrochemistry. *Angew Chem. Int. Ed.* **63**, e202319246 (2024).
11. Yang, M. C. et al. Reduced graphene oxide nanosheets decorated with core-shell of Fe3O4-Au nanoparticles for rapid SERS detection and hyperthermia treatment of bacteria. *Spectrochim Acta Part. A: Mol. Biomol. Spectrosc.* **281**, 121578 (2022).
12. Cao, X. et al. Detection of neonicotinoids in agricultural products using magnetic molecularly imprinted polymers-surface enhanced Raman spectroscopy. *Talanta*. **266**, 125000 (2024).
13. Juang, R. S. et al. Fabrication of in situ magnetic capturing and Raman enhancing nanoplatelets for detection of bacteria and biomolecules. *Colloids Surf. A: Physicochem Eng. Asp*. **648**, 129189 (2022).
14. Su, D. S., Tsai, D. P., Yen, T. J. & Tanaka, T. Ultrasensitive and Selective Gas Sensor based on a Channel Plasmonic structure with an enormous hot Spot Region. *Acs Sens.* **4**, 2900–2907 (2019).
15. Rauh, F., Dittloff, J., Thun, M., Stutzmann, M. & Sharp, I. D. Nanostructured Black Silicon as a stable and surface-sensitive platform for time-resolved in situ Electrochemical Infrared absorption spectroscopy. *ACS Appl. Mater. Interfaces*. **16**, 6653–6664 (2024).
16. Jiang, R. et al. Engineering Near-Infrared Plasmonic Spiky Gold nanostructures for highly efficient surface-enhanced Raman Spectroscopy-guided Cancer Hyperthermia Therapy. *Adv. Funct. Mater.* **34**, (2024).

17. Kalachyova, Y. et al. Surface Plasmon Polaritons on Silver Gratings for Optimal SERS Response. *J. Phys. Chem. C.* **119**, 9506–9512 (2015).
18. Autore, M., Mester, L., Goikoetxea, M. & Hillenbrand, R. Substrate matters: surface-polariton enhanced Infrared Nanospectroscopy of Molecular vibrations. *Nano Lett.* **19**, 8066–8073 (2019).
19. Chen, X. et al. All-dielectric metasurfaces with high Q-factor Fano resonances enabling multi-scenario sensing. *Nanophotonics.* **11**, 4537–4549 (2022).
20. Cheng, F., Yang, X. & Gao, J. Ultrasensitive detection and characterization of molecules with infrared plasmonic metamaterials. *Sci. Rep-uk.* **5**, 14327 (2015).
21. Kumar, S. R. P., Mitra, A. & R. & Electrically reconfigurable phase change material-based Metamaterial Absorber for Broadband Molecular Fingerprint Retrieval. *ACS Photonics.* **11**, 1793–1803 (2024).
22. Sayed, S. I., Mahmoud, K. R. & Mubarak, R. I. Design and optimization of broadband metamaterial absorber based on manganese for visible applications. *Sci. Rep.* **13**, 11937 (2023).
23. Lu, C. Y., Chung, C. C., Yen, T. J. & Huang, T. Y. Achieving broad absorption band and high incident angles by stochastically-distributed oblique-flat-sheet metamaterial perfect absorbers. *Sci. Rep-uk.* **11**, 18713 (2021).
24. Wu, X. X., Lu, C. Y. & Huang, T. Y. Creating hot spots within air for better sensitivity through design of oblique-wire-bundle metamaterial perfect absorbers. *Sci. Rep-uk.* **12**, 3557 (2022).
25. Jensen, M. O. & Brett, M. J. Periodically structured glancing Angle Deposition Thin films. *Ieee T Nanotechnol.* **4**, 269–277 (2005).

Acknowledgements
The authors acknowledge the financial support from National Science and Technology Council (NSTC 113-2221-E-131-019) and from the Center for Plasma and Thin Film and Thin Film Technologies and Ming Chi University of Technology.

Author contributions
T. Y. H. conceived the project, T. Y. H. , H. S. L. and C. Y. L. designed and simulated the sample. T. Y. H.and Y. P. K. measured the sample. T. Y. H., H. S. L. and C. Y. L. co-wrote the paper. All authors discussed the results and commented on the manuscript.

Declarations

Competing interests
The authors declare no competing interests.

Additional information
Correspondence and requests for materials should be addressed to T.-Y.H.